Turbulence Unsteadiness Drives Extreme Clustering

F. Zapata,[1,2,*] S. Angriman,[1,2] A. Ferran,[3,4] P. Cobelli,[1,2] M. Obligado,[3] and P. D. Mininni[1,2]

[1]*Universidad de Buenos Aires, Facultad de Ciencias Exactas y Naturales, Departamento de Física, Ciudad Universitaria, 1428 Buenos Aires, Argentina*

[2]*CONICET—Universidad de Buenos Aires, Instituto de Física Interdisciplinaria y Aplicada (INFINA), Ciudad Universitaria, 1428 Buenos Aires, Argentina*

[3]*Université Grenoble Alpes, CNRS, Grenoble-INP, LEGI, F-38000 Grenoble, France*

[4]*Department of Mechanical Engineering, University of Washington, Seattle, Washington 98195-2600, USA*

(Received 29 September 2023; accepted 13 February 2024; published 8 March 2024)

We show that the unsteadiness of turbulence has a drastic effect on turbulence parameters and in particle cluster formation. To this end we use direct numerical simulations of particle laden flows with a steady forcing that generates an unsteady large-scale flow. Particle clustering correlates with the instantaneous Taylor-based flow Reynolds number, and anticorrelates with its instantaneous turbulent energy dissipation constant. A dimensional argument for these correlations is presented. In natural flows, unsteadiness can result in extreme particle clustering, which is stronger than the clustering expected from averaged inertial turbulence effects.

DOI: 10.1103/PhysRevLett.132.104005

One of the most counterintuitive effects of turbulence is that, when a fluid is loaded with inertial particles, the flow can segregate the particles instead of mixing them [1,2]. This phenomenon, which results in the formation of clusters with enhanced particle density, is relevant in volcanic clouds [3,4], to explain cloud formation [5] and electrification [6], in other geophysical and natural contexts [7], and for industrial applications. In homogeneous and isotropic turbulence, two mechanisms govern the formation of clusters: particles with small inertia are expelled out of vortices [8], while particles with large inertia accumulate near points with zero net forces [9].

Turbulence is an out-of-equilibrium phenomenon that is often studied in the statistical steady state, i.e., when external forces and dissipation balance in such a way that the system has well defined time averages. However, in many natural and industrial systems this is not the case. Out-of-equilibrium systems can fluctuate randomly between two or more states, in such a way that time averages never converge [10]. Unsteadiness affects energy dissipation rates and the flow spectral properties [11]. This in turn has an effect in the mixing and transport of particles. As an example, it has been reported that motile particles such as phytoplankton can change their direction of migration in response to overturning events associated to the turbulent flow in which they move [12].

What is the effect of unsteadiness in passive particles' cluster formation? And is the formation and evolution of clusters in realistic flows driven by turbulence, by the flow unsteadiness, or by a combination of both? Here, we show that the naturally occurring modulation of out-of-equilibrium systems in time has a drastic effect on turbulence parameters and in particle cluster formation. Moreover, we show that clustering correlates with a small time delay with the instantaneous Taylor-based Reynolds number of the flow, and anticorrelates with its instantaneous turbulent energy dissipation rate. Hysteresis is present in this process, indicating the particles preserve a memory of previous states. We present a dimensional argument that considers this phenomenon as a change in the particles' effective inertia (measured by the Stokes number) depending on the flow state. This result allows for estimation of turbulent parameters from particles measurements, and indicates that flow unsteadiness must be considered in the study of many multiphase flows.

We performed direct numerical simulations (DNSs) of the incompressible Navier-Stokes equation

$$\partial_t \mathbf{u} + \mathbf{u} \cdot \boldsymbol{\nabla} \mathbf{u} = -\boldsymbol{\nabla} p + \nu \nabla^2 \mathbf{u} + \mathbf{F}, \tag{1}$$

where $\mathbf{u}$ is the solenoidal fluid velocity field ($\nabla \cdot \mathbf{u} = 0$), p is the pressure per unit mass density, ν is the kinematic viscosity, and $\mathbf{F}$ is an external volumetric mechanical forcing. Equations are written in dimensionless units based on a unit length L_0 and a unit velocity U_0, and solved in a three-dimensional $2\pi L_0$-periodic cubic box with a parallel pseudospectral method using the GHOST code [13,14]. Spatial resolutions of $N^3 = 512^3$, 768^3, and 1024^3 grid points were used, yielding increasingly larger Reynolds numbers with kinematic viscosities respectively of $\nu_{512} = 1.1 \times 10^{-3} L_0 U_0$, $\nu_{768} = 6.7 \times 10^{-4} L_0 U_0$, and $\nu_{1024} = 4.6 \times 10^{-4} L_0 U_0$. The external forcing $\mathbf{F}$ generates large-scale periodic counter-rotating columns (in the following abbreviated as CRCs). It was used before to study unsteadiness in [15], and is given by

$$\mathbf{F} = F_0[\sin(x)\cos(y)\hat{x} - \cos(x)\sin(y)\hat{y}]. \qquad (2)$$

This forcing corresponds to an array of four counter-rotating vortices in the xy plane, with translational symmetry in z. The first columnar vortex occupies the volume $[0, \pi L_0) \times [0, \pi L_0) \times [0, 2\pi L_0)$, and is separated from the others by two vertical shear layers in the middle of the domain, aligned respectively with the xy and xz planes.

We also performed DNSs of homogeneous and isotropic turbulence (HIT) with random forcing, to compare against the CRC runs, following the same procedures used for the CRC forcing and using $N^3 = 768^3$ and 1024^3 grid points. In these simulations the flow was sustained using a forcing with fixed amplitude and random phases, which were slowly evolved in time with a correlation time of 0.5 large-scale eddy turnover times to prevent the development of a mean flow. The forcing was applied at the lowest wave numbers, resulting in an integral length scale $L \approx 1.1 L_0$. The kinematic viscosities were $\nu_{768} = 3.1 \times 10^{-4} L_0 U_0$ and $\nu_{1024} = 2.1 \times 10^{-4} L_0 U_0$. A DNS similar to HIT, but with time dependent forcing amplitude to synthetically generate unsteadiness, is discussed in [16]. All simulations have $\kappa\eta > 1$, where $\kappa = N/3$ is the largest resolved wave number, $\eta = (\nu^3/\varepsilon)^{1/4}$ is the dissipation scale, and ε is the energy dissipation rate.

In all simulations we integrated a simple model of one way coupled and heavy point particles with equation of motion

$$\dot{\mathbf{x}}_p = \mathbf{v}(t), \qquad \dot{\mathbf{v}} = \frac{1}{\tau_p}[\mathbf{u}(\mathbf{x}_p, t) - \mathbf{v}(t)], \qquad (3)$$

where $\mathbf{u}(\mathbf{x}_p, t)$ is the fluid velocity at the particle position $\mathbf{x}_p$ at time t, and $\mathbf{v}(t)$ and τ_p are respectively the particle velocity and the particle Stokes time. In each run different sets of particles were added, each with 10^6 particles and with different values of τ_p. The Stokes (St) numbers of these sets, $\mathrm{St} = \tau_p/\tau_\eta$ (where $\tau_\eta = (\nu/\varepsilon)^{1/2}$ is the Kolmogorov dissipation time of the flow), were St = 3 and 8 for all flows and all spatial resolutions considered. A third set with St = 14 was also evolved only in the simulations with 1024^3 grid points. For the CRC runs, τ_η and St are the time average over very long times.

The overall dynamics of the flows is as follows. While the HIT simulations display fluctuations in global quantities with a correlation time proportional to the integral turnover time, the CRC runs display distinct dynamics. Large excursions in the energy dissipation and other global quantities are observed, resulting from the flow transitioning from two states: one in which the large-scale columns can be clearly recognized (e.g., by direct inspection of the instantaneous spatial distribution of particles), and one in which the columns become unstable and the system displays a more homogeneous state. A movie of this time evolution can be seen in [16].

An out-of-equilibrium dissipation law has been reported in a variety of unsteady turbulent flows [17,18], such that

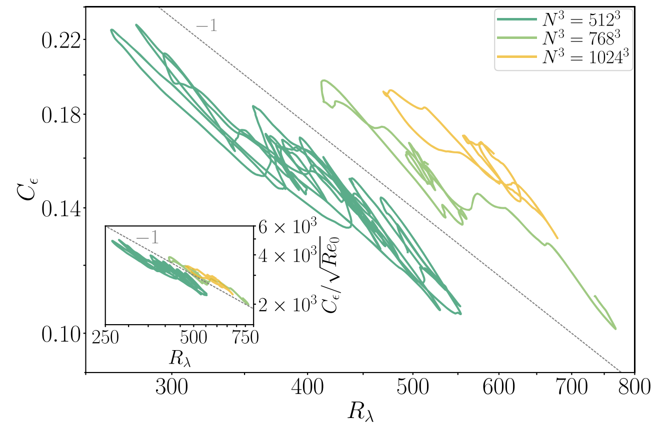

FIG. 1. Instantaneous value of C_ε as a function of R_λ for the CRC flow at three different spatial resolutions. Each resolution corresponds to a different viscosity and to a different averaged Reynolds number. Inset: C_ε compensated by $\sqrt{\mathrm{Re}_0}$ as a function of R_λ.

$$C_\varepsilon \sim \frac{\sqrt{\mathrm{Re}_0}}{R_\lambda}, \qquad (4)$$

where $\mathrm{Re}_0 = u_0 l_0/\nu$ is a global Reynolds number based on the initial rms flow velocity u_0 and the initial integral length scale l_0, and $R_\lambda = u(t)\lambda(t)/\nu$ is the local-in-time Reynolds number based on the instantaneous Taylor length scale $\lambda(t)$ and rms turbulent velocity $u(t)$. C_ε is given by the energy dissipation rate as $\varepsilon(t) = C_\varepsilon u^3(t)/L(t)$, where $L(t)$ is the instantaneous flow integral scale. For a turbulent steady state (e.g., in HIT) this relation reduces to the well-known dissipation law $\varepsilon = C_\varepsilon u^3/L$ that states that the energy dissipation rate is governed by the large-scale energy flux toward smaller scales. In this sense, in unsteady flows $C_\varepsilon(t)$ provides a measure of temporal scale-by-scale energy imbalance.

In Fig. 1 we see that the CRC flows display excursions compatible with Eq. (4) as C_ε is inversely proportional to R_λ. In the inset we show C_ε compensated by the square root of the reference Reynolds number Re_0; note how all curves from flows with different viscosities collapse. For a given viscosity (e.g., for $N^3 = 512^3$) R_λ and C_ε change in time by factors of 2, with a typical timescale of the excursions of $10\langle T\rangle$ to $20\langle T\rangle$, where $\langle T\rangle$ is the mean large-scale eddy turnover time (see details below). These excursions, as well as their characteristic timescale, are much larger than those associated to the fluctuations in simulations of HIT (which take place in timescales of the order of the turnover time). In spite of these differences, the instantaneous energy spectrum of the CRC simulations still displays Kolmogorov scaling (not shown).

We want to know if these excursions in the dissipation and in the Taylor-based Reynolds number, similar to those reported in other unsteady turbulent flows [15,17,18], affect particle cluster formation and time evolution. To estimate

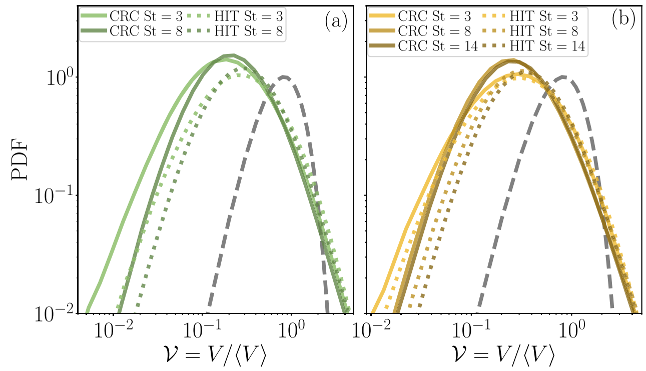

FIG. 2. Probability density functions (PDFs) of the normalized Voronoï volumes $\mathcal{V} = V/\langle V \rangle$ of inertial particles for CRC and HIT simulations, for (a) $N^3 = 768^3$, and (b) $N^3 = 1024^3$. For CRC forcing, the PDFs are time-averaged over long times. A random Poisson process (RPP) is indicated by the dashed line.

the amount of clustering in the different simulations we calculated the three-dimensional Voronoï tessellation of the particles as a function of time. Voronoï diagrams have proven to be a powerful tool to study particle clustering [19,20]. The Voronoï cell associated to a given particle at a certain time is defined as the set of points closer to that particle than to any other particle. The volumes of the Voronoï cells V were normalized by the mean volume of all cells $\langle V \rangle$, to define normalized volumes $\mathcal{V} = V/\langle V \rangle$. Figure 2 shows the time-averaged probability density functions (PDFs) of the normalized volumes, compared against the PDF resulting from a random Poisson process (herein RPP, corresponding to a homogeneous distribution of particles [21]), which is shown as a reference. The stronger the tails of the PDFs compared against the RPP (i.e., the excess of probability for small $\mathcal{V}$ corresponding to an excess of small volumes, or for large $\mathcal{V}$ corresponding to large voids), and the larger the standard deviation of the PDFs, $\sigma_{\mathcal{V}}$ compared to the RPP (which has a standard deviation of $\sigma_{\mathrm{RPP}} \approx 0.42$), the stronger the clustering. Positions of the maxima also change as variables in the PDFs are normalized to obtain mean volumes occupied per particle.

As shown in Fig. 2, the CRC runs present stronger clustering than HIT, when comparing cases with the same Stokes number. As St increases (at fixed spatial resolution) clustering diminishes, indicating that particles with more inertia cluster less both in CRC and HIT flows (results presented here are for $\mathrm{St} \gtrsim 1$, as for $\mathrm{St} \to 0$ and $\to \infty$ particles do not cluster; note that in the CRC flow for $\mathrm{St} = 14$ clustering is similar to $\mathrm{St} = 8$ and less than for 3). Differences between the CRC flow and HIT could in principle be associated with the presence of a large-scale flow in the CRC runs, but this is not sufficient to explain the observed enhancement in clustering. In other turbulent flows with a steady large-scale circulation, particle clustering was observed to be closer to that of HIT [22]. The reason for the stronger clustering here becomes more clear when inspecting the instantaneous PDFs of $\mathcal{V}$. Note that all PDFs in Fig. 2 are averaged over a time window of $\approx 5\langle T \rangle$, using 10^6 Voronoï volumes in each snapshot with a cadence of at least $0.04\langle T \rangle$. But while the PDFs of $\mathcal{V}$ in HIT are stationary, the PDFs in the CRC runs are not (see a movie with the PDFs as a function of time in [16]).

The instantaneous PDFs of the CRC flow vary significantly in time, and the time-averaged PDFs showed in Fig. 2 alone are not representative of the actual level of particle clustering. To study how particle clustering is affected by the flow unsteadiness, we calculated the time evolution of C_ε, ε, R_λ, and the standard deviation of the Voronoï volumes, $\sigma_{\mathcal{V}}$. Results are shown in Fig. 3. Particles are injected when the flows are already in a fully developed turbulent regime, at a time arbitrarily labeled as $t = 0$, and at random positions in space (note that at $t = 0$, $\sigma_{\mathcal{V}} = \sigma_{\mathrm{RPP}}$ in all cases). After a short transient, particles form clusters as indicated by $\sigma_{\mathcal{V}} > \sigma_{\mathrm{RPP}}$. It has been reported before [15] that this flow displays irregular behavior of large-scale quantities. Our results for C_ε and R_λ are compatible with this observation: both quantities display large excursions with a characteristic timescale much larger than the integral turnover time. Fluctuations in C_ε have a correlation time between $10\langle T \rangle$ to $20\langle T \rangle$, and result in fluctuations of the flow dissipation rate ε with a similar characteristic time. More surprising are the fluctuations in $\sigma_{\mathcal{V}}$, which can vary between ≈ 2.5 to values larger than 6, indicating strong variations in the level of particle clustering as the flow evolves.

Comparing the four quantities in Fig. 3 we see that when C_ε and ε display a local minimum, R_λ and $\sigma_{\mathcal{V}}$ display local maxima (i.e., turbulence becomes stronger and particles cluster more). To quantify the correlation between clustering and R_λ, the cross-correlation function f_{corr} of $\sigma_{\mathcal{V}}$ and R_λ is shown in an inset in Fig. 3, for the simulation with 512^5 grid points as this simulation has the longest integration in time. The maximum cross-correlation is reached for time increments $|\tau|/\langle T \rangle \lesssim 1$ (negative increments are associated to particles clustering during the growth of R_λ). Similar results are obtained when the cross-correlation is computed with C_ε. Thus, C_ε or R_λ and $\sigma_{\mathcal{V}}$ are correlated with a time lag that is proportional to the large-scale eddy turnover time. The existence of this time lag suggests that the response of the particles to changes in flow properties may display hysteresis.

Figure 4 shows $\sigma_{\mathcal{V}}$ as a function of R_λ in CRC runs, for particles with $\mathrm{St} = 3$ and 8, and for different viscosities and spatial resolutions. Time intervals with increasing R_λ are marked with solid lines, while intervals with decreasing R_λ are indicated with dashed lines. The figure indicates a Reynolds number dependence, and further confirms the correlation between these quantities and the existence of a time lag with a hysteresis cycle superposed over the strong fluctuations.

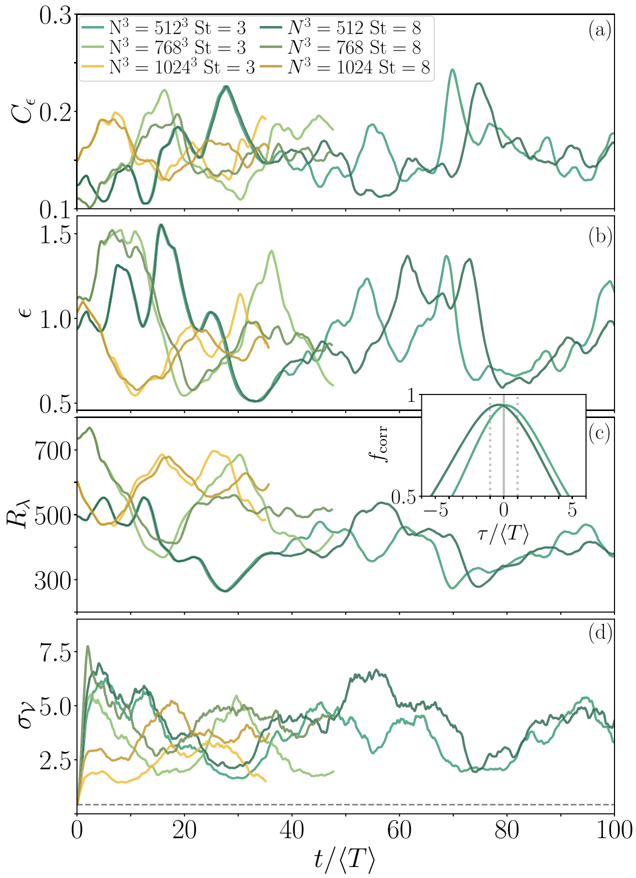

FIG. 3. Time series of (a) C_ε, (b) ε, (c) R_λ, and (d) $\sigma_\mathcal{V}$ for CRC runs with St = 3 and 8. Time is normalized by the mean turnover time $\langle T\rangle$, and σ_{RPP} is indicated by the dotted gray line in panel (d). Inset: cross-correlation of $\sigma_\mathcal{V}$ and R_λ as a function of the time lag τ.

As previously mentioned, this level of particle clustering and its fluctuations are stronger than in HIT. Figure 5 compares the PDFs of $\sigma_\mathcal{V}$ for CRC forcing and for HIT, in the case with $N^3 = 768^3$ and St = 8. The two flows display distinct values of $\sigma_\mathcal{V}$. In HIT $\sigma_\mathcal{V}$ takes values between 0.5 and 1.8, while in the CRC flow values go from 0.5 to 7.4, reaching its maximum value around ≈4.5. Not only is $\sigma_\mathcal{V}$ on average significantly larger in the CRC flow (i.e., particles cluster more), but the dispersion in the values of $\sigma_\mathcal{V}$ is also much larger, including instances (albeit less probable) in which the clustering is similar to that found in HIT, as the ones captured by the left tail of the PDF. The dispersion in $\sigma_\mathcal{V}$, and the correlation with R_λ, confirm that the extreme clustering observed in this flow is associated to its unsteady dynamics (see also [16]).

How does the out-of-equilibrium dynamics of the flow affect the particle behavior? We can consider first the situation in which turbulence is in a scale-by-scale steady state. Under these conditions, $\mathrm{Re}_0 = u_0 l_0/\nu \approx uL/\nu$ (where $u = \langle u(t)\rangle$ is the time average of the rms flow velocity, and $L = \langle L(t)\rangle$ is the averaged flow integral scale). The energy dissipation rate is also $\varepsilon \approx u^3/L$. For a small spherical particle we can write the Stokes time as $\tau_p = 2a^2\rho_p/(9\rho_f\nu)$ (where a is the particle radius, ρ_p is the particle density, and ρ_f is the fluid density). Then $\mathrm{St} = \tau_p/\tau_\eta = (2/9)(\rho_p/\rho_f)(a/L)^2\mathrm{Re}_0^{3/2}$. Thus, the Stokes number of the particles (and as a result, the sensitivity of the particles to flow fluctuations at different scales) is fixed given a particle radius, a mass density ratio, and a flow Reynolds number. However, when scale-by-scale steadiness is broken, we must use $\varepsilon = C_\varepsilon U^3/L$, which using Eq. (4) results in $\mathrm{St} \sim (2/9)(\rho_p/\rho_f)(a/L)^2\mathrm{Re}_0^{7/4}/R_\lambda^{1/2}$. The sensitivity of the

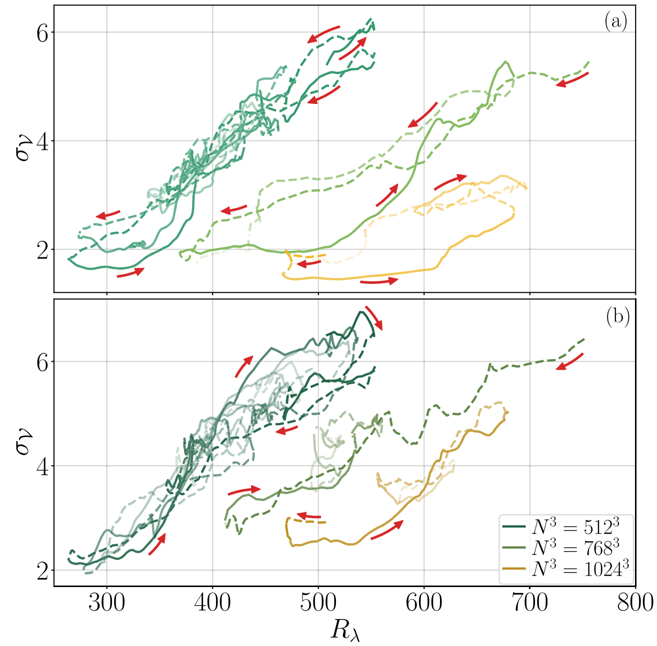

FIG. 4. Standard deviation of the Voronoi volumes, $\sigma_\mathcal{V}$, as a function of R_λ for CRC runs, differentiating branches in which R_λ increases (solid lines) and decreases (dashed lines), for (a) St = 3, and (b) 8. Red arrows indicate the direction of time evolution.

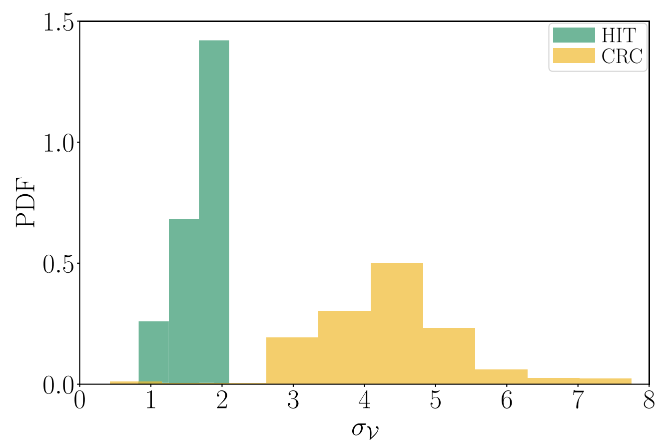

FIG. 5. PDFs of $\sigma_\mathcal{V}$ for HIT and CRC runs with $N^3 = 768^3$ and for particles with St = 8. Note the larger values of $\sigma_\mathcal{V}$ (i.e., enhanced clustering) in the CRC run, as well as the larger dispersion.

particles to flow fluctuations thus changes depending on the instantaneous dissipation (or the Taylor-based Reynolds number). Equivalently, we could interpret this expression as the effective ratio of the particle size to the flow scale being replaced by $a/(LR_\lambda^{1/4})$: the integral scale of the flow "seen" by the particle depends on R_λ. Perhaps counterintuitively, for larger R_λ the particles become more sensitive to the larger scale eddies, which results in stronger clustering, as can be seen in the movie in [16]. When R_λ is smaller (C_ε larger) the effective Stokes number of the particles is larger and the spatial distribution of particles is more homogeneous, with clustering closer to that observed in inertial clustering in HIT. When R_λ is larger (C_ε smaller), St is smaller, and particles accumulate outside the large-scale columnar vortices in a phenomenon reminiscent of turbophoresis (i.e., expelled from the vortices [8]), resulting in extreme clusterization. As discussed previously, this argument can hold for St larger than 1 but in its vicinity, as considered in our simulations.

Natural flows are unsteady: volcanic and other sources of particulate material pulsate and oscillate in time, convection in clouds is inhomogeneous, and atmospheric turbulence in general is bursty [23]. The results presented here show that flow unsteadiness, which in this case occurs naturally as a steady forcing is used, can drastically enhance particle clustering, well above what previous studies have reported for steady state homogeneous and isotropic turbulence. Thus this effect, which has been neglected so far, can change estimations of clustering and particle aggregation for many systems. As an example, estimations of collision frequencies between particles are proportional to $n^2 \sim \mathcal{V}^{-2}$ (where n is the particle density), and changes in the volume per particle $\mathcal{V}$ affect the number of collisions. The results also open the door to the estimation of instantaneous turbulence parameters from direct observations of particle aggregation (albeit taking into account that the dependence on Re_0 could be different for different flows), and can be useful for the study of other out-of-equilibrium unsteady systems.

This work has been partially supported by Evaluation-orientation de la COopération Scientifique (ECOS-Sud) Project No. A18ST04. F. Z., S. A., P. C., and P. D. M. acknowledge financial support from UBACyT Grant No. 20020170100508BA and Proyectos de Investigación Científica y Tecnológica (PICT) Grant No. 2018-4298. A. F. and M. O. acknowledge the LabEx Tec21 (Investissements d'Avenir—Grant Agreement No. ANR-11-LABX-0030).

*Corresponding author: fnzapata@df.uba.ar

[1] L. Brandt and F. Coletti, Annu. Rev. Fluid Mech. **54**, 159 (2022).

[2] M. Obligado, T. Teitelbaum, A. Cartellier, P. D. Mininni, and M. Bourgoin, J. Turbul. **15**, 293 (2014).

[3] T. Esposti Ongaro and M. Cerminara, J. Volcanol. Geotherm. Res. **326**, 127 (2016).

[4] M. Ichihara, P. D. Mininni, S. Ravichandran, C. Cimarelli, and C. Vagasky, Commun. Earth Environ. **4**, 417 (2023).

[5] R. A. Shaw, Annu. Rev. Fluid Mech. **35**, 183 (2003).

[6] M. Di Renzo and J. Urzay, Nat. Commun. **9**, 1676 (2018).

[7] R. E. Breier, C. C. Lalescu, D. Waas, M. Wilczek, and M. G. Mazza, Proc. Natl. Acad. Sci. U.S.A. **115**, 12112 (2018).

[8] L.-P. Wang and M. R. Maxey, J. Fluid Mech. **256**, 27 (1993).

[9] S. Coleman and J. Vassilicos, Phys. Fluids **21**, 113301 (2009).

[10] A. de la Torre and J. Burguete, Phys. Rev. Lett. **99**, 054101 (2007).

[11] S. Berti, G. Boffetta, and S. Musacchio, Phys. Rev. Fluids **8**, 054601 (2023).

[12] A. Sengupta, F. Carrara, and R. Stocker, Nature (London) **543**, 555 (2017).

[13] P. D. Mininni, D. Rosenberg, R. Reddy, and A. Pouquet, Parallel Comput. **37**, 316 (2011).

[14] D. Rosenberg, P. D. Mininni, R. Reddy, and A. Pouquet, Atmosphere **11**, 178 (2020).

[15] S. Goto and J. Vassilicos, Phys. Lett. A **379**, 1144 (2015).

[16] See Supplemental Material at http://link.aps.org/supplemental/10.1103/PhysRevLett.132.104005 for the analysis of a third forcing that synthetically generates unsteadiness in an isotropic and homogeneous setup, and for a movie showing the time evolution of the CRC flow and the statistics of the particles.

[17] P. C. Valente, R. Onishi, and C. B. da Silva, Phys. Rev. E **90**, 023003 (2014).

[18] J. C. Vassilicos, Atmosphere **14**, 736 (2023).

[19] R. Monchaux, M. Bourgoin, and A. Cartellier, Phys. Fluids **22** (2010).

[20] R. Monchaux, M. Bourgoin, and A. Cartellier, Int. J. Multiphase Flow **40**, 1 (2012).

[21] M. Uhlmann, Physica (Amsterdam) **555A**, 124618 (2020).

[22] S. Angriman, A. Ferran, F. Zapata, P. J. Cobelli, M. Obligado, and P. D. Mininni, J. Fluid Mech. **948**, A30 (2022).

[23] P. R. Imazio, P. D. Mininni, A. Godoy, N. Rivaben, and A. Dörnbrack, J. Geophys. Res. **128**, e2022JD037491 (2023).